DALTON
FULL PAPER

2,5-Bis(1-phenyliminoethyl)pyrazine (bpip): a conjugated metal–metal bridging acceptor ligand and its homodinuclear complexes with low-valent metal centres

Axel Klein,[a] Volker Kasack,[a] Ralf Reinhardt,[a] Torsten Sixt,[a] Thomas Scheiring,[a] Stanislav Zalis,[b] Jan Fiedler[b] and Wolfgang Kaim*[a]

[a] *Institut für Anorganische Chemie, Universität Stuttgart, Pfaffenwaldring 55, D-70550 Stuttgart, Germany*
[b] *J. Heyrovsky Institute of Physical Chemistry, Academy of Sciences of the Czech Republic, Dolejškova 3, CZ-18223 Prague, Czech Republic*

Received 26th October 1998, Accepted 21st December 1998

Complexes of 2,5-bis(1-phenyliminoethyl)pyrazine (bpip), a symmetrical bis(bidentate) ligand which acts through two different chelate donor centres, one imine and one azine nitrogen atom per metal chelate site, have readily been obtained with $Cr(CO)_4$, $Mo(CO)_4$, $W(CO)_4$, $Mn(CO)_3Cl$, $Re(CO)_3Cl$, $[Ru(bpy)_2]^{2+}$ and $[Cu(PPh_3)_2]^+$ fragments. The 'free' ligand and the dinuclear $[\{Cu(PPh_3)_2\}_2(\mu\text{-bpip})][BF_4]_2$ were characterised crystallographically. The low-energy molecular conformation of free bpip is qualitatively different from the planar *syn*/*trans*/*syn* arrangement required in the bpip-bridged dicopper(I) compound (Cu · · · Cu distance 6.944 Å). Structural preferences and the π acceptor properties of the conjugated bridging ligand bpip were studied using DFT calculations of the $bpip^{0/-/2-}$ chromophore and combined electrochemical and spectroscopic methods; bpip is a stronger π acceptor than the related 2,5-bis(2-pyridyl)pyrazine but a poorer mediator of metal–metal interaction.

Conjugated bridging ligands with low-lying unoccupied molecular orbitals are sought after materials in various areas of supramolecular and co-ordination chemistry. Such molecules can support the formation of dendrimers and co-ordination polymers,[1] mediate magnetic interactions between metal centres,[2] give rise to mixed-valent dimers,[3] show low-lying charge transfer excited states,[4] facilitate energy or electron transfer between the bridged metal centres,[1a,c,3,5] and exhibit a rich electrochemistry.[6] While $\mu\text{-}\eta^1:\eta^1$ co-ordinating ligands such as pyrazine or 4,4′-bipyridine are quite useful in that respect,[7] the superior stability of complexes with bis(chelating) bridging ligands ($\mu\text{-}\eta^2:\eta^2$) is more helpful in the construction of robust materials. For instance, co-ordinating bis(chelate) ligands with "S frame"[2c] conformation such as 2,5-bis(2-pyridyl)pyrazine (2,5-dpp also abbreviated as bppz or dppz) have been much used recently in assembling oligonuclear compounds for the purpose of light-induced energy transfer.[1a]

While 2,5-dpp can be considered as a replicated 2,2′-bipyridine ligand with potentially conjugating aromatic rings, the previously used[8–10] and partially characterised[11] bis(chelating) acceptor 2,5-bis(1-phenyliminoethyl)pyrazine (bpip) may be viewed as a centrosymmetrically replicated 2-pyridinecarbaldimine (pyca)[11–17] system. As imine/azine hybrid chelating systems the pyca and bpip ligands contain the more flexible non-aromatic CR′=NR groups which can bear different kinds of substituents; related to bpip is 2,5-bis(4-dimethylaminophenyliminomethyl)pyrazine which contains strongly electron-donating aryl groups as nitrogen substituents.[18] Other attempts to couple 2-pyridinecarbaldimine moieties involved the insertion of potentially conjugating aromatics,[5b,6a] however, such systems contain a large number of π centers which usually diminishes the potential for metal–metal interaction.

In this work we describe the crystal structure of the bpip ligand, its spectroelectrochemistry, and DFT calculation results for neutral, anionic and dianionic states of bpip′ = 2,5-bis(1-phenyliminomethyl)pyrazine. Mononuclear $[Re(bpip)(CO)_3Cl]$ and homodinuclear complexes with low-valent metal complex fragments $M(CO)_4$ (M = Cr, Mo or W), $M'(CO)_3Cl$ (M′ = Mn or Re), $[Ru(bpy)_2]^{2+}$ and $[Cu(PPh_3)_2]^+$ are presented, including a crystal structure of $[\{Cu(PPh_3)_2\}_2(\mu\text{-bpip})][BF_4]_2$. The electronic situation in the complexes was studied by means of cyclic voltammetry, absorption spectroscopy (solvatochromism, spectroelectrochemistry) and EPR of reduced forms. Homodinuclear co-ordination compounds of bpip with other metal centres have been reported, involving $Rh^{I,II,III}$, $Ir^{I,II,III}$,[9] $Pt^{II,III,IV}$[10] and Mg^{II}.[11] The redox system $[\{Ru(bpy)_2\}_2(bpip)]^{n+}$ was referred to in an earlier EPR study.[8]

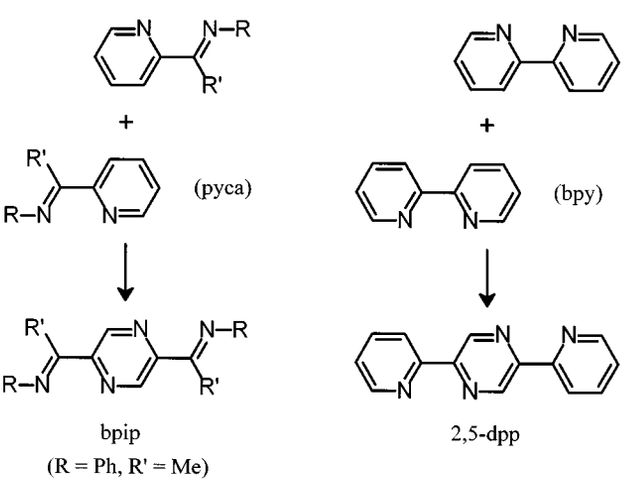

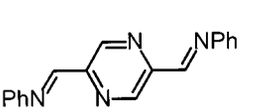

bpip′

Table 1 Carbonyl stretching frequencies $\tilde{\nu}$ of complexes[a]

Compound	$\tilde{\nu}_{C-O}/cm^{-1}$		
$[\{Cr(CO)_4\}_2(\mu\text{-bpip})]$	1989vs	1918vs	1863s
$[\{Mo(CO)_4\}_2(\mu\text{-bpip})]$	2000vs	1920vs	1865s
$[\{W(CO)_4\}_2(\mu\text{-bpip})]$	1986vs	1909vs	1860s
$[\{Mn(CO)_3Cl\}_2(\mu\text{-bpip})]$	2025s	1945s	1910vs
$[Re(bpip)(CO)_3Cl]$	2027vs	1934s	1905s
$[\{Re(CO)_3Cl\}_2(\mu\text{-bpip})]$	2020vs	1940s	1910s

[a] Measured in THF solution.

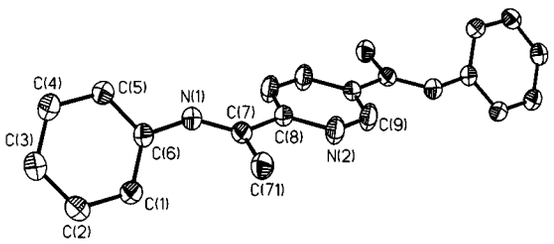

Fig. 1 Molecular structure of bpip in the crystal.

Results and discussion

Synthesis and characterisation

The compound bpip was obtained from aniline and 2,5-diacetylpyrazine in hexane, using acidic alumina as catalyst and molecular sieve for dehydration.[11] Primary alkylamines did not react under such conditions or in the benzene–toluene-*p*-sulfonic acid system. Thermal reactions of the photogenerated solvates $[M(THF)(CO)_5]$ (M = Cr, Mo or W) with bpip produced the bis(tetracarbonylmetal) complexes; in the case of M = Mo, the use of the tetracarbonyl(norbornadiene)molybdenum precursor gave better yields. Typically, mononuclear complexes could not be isolated even with an excess of bpip although intermediate colouration was observed *e.g.* in the reaction with $[W(THF)(CO)_5]$. In the thermal reaction between bpip and 2 molar equivalents of $[Re(CO)_5Cl]$ in toluene[19] the intermediate red colour before the appearance of the blue dinuclear complex is attributed to a mononuclear species $[Re(bpip)(CO)_3Cl]$ which was subsequently synthesized separately and studied for comparison with the dinuclear compound.

The dinuclear compounds of Mn^{I}, Cu^{I} and Ru^{II} were prepared according to standard procedures;[19–21] the isolated diruthenium complex was found to contain varying amounts of the one-electron reduced form.

The metal carbonyl compounds exhibit typical CO stretching bands in the infrared region (Table 1). The compound bpip and $[\{Cu(PPh_3)_2\}_2(\mu\text{-bpip})][BF_4]_2$ could be characterised crystallographically.

Crystal structures of bpip and $[\{Cu(PPh_3)_2\}_2(\mu\text{-bpip})][BF_4]_2$ and DFT calculations

Both molecules bpip and $[\{Cu(PPh_3)_2\}_2(\mu\text{-bpip})][BF_4]_2$ exhibit inversion symmetry in the respective crystals; significant intermolecular interactions were not observed. The crystal data and structural results are summarised in Tables 2 and 3 and the molecular structures are illustrated by Figs. 1 and 2.

A main difference between the conformations of free and metal–metal bridging bpip lies in the co-ordination-induced *syn*/*trans*/*syn* arrangement **III** as observed here for the dicopper complex (Fig. 2) whereas unco-ordinated bpip adopts a lower-energy form, an *anti*/*trans*/*anti* conformation **I** of the virtually planar bis(iminoethyl)pyrazine π system with significantly (54.9°) tilted phenyl rings (Fig. 1). Owing to the sterically demanding metal complex fragments the tilt angle increases to 89.3° in the dicopper complex in which the imine functions adopt a *ca*. 10° dihedral angle with respect to the pyrazine ring.

Table 2 Selected distances (Å) and bond angles (°) of bpip in the crystal

C(6)–N(1)	1.419(2)	C(8)–N(2)	1.336(2)
C(7)–N(1)	1.279(2)	C(8)–C(9A)	1.392(2)
C(7)–C(8)	1.489(2)	C(9)–N(2)	1.331(2)
C(7)–C(71)	1.501(2)		
C(5)–C(6)–N(1)	117.54(12)	N(2)–C(8)–C(7)	117.33(13)
C(1)–C(6)–N(1)	122.57(13)	C(9A)–C(8)–C(7)	122.25(12)
N(1)–C(7)–C(8)	116.00(13)	N(2)–C(9)–C(8A)	122.69(13)
N(1)–C(7)–C(71)	127.10(13)	C(7)–N(1)–C(6)	121.94(12)
N(2)–C(8)–C(9A)	120.40(13)	C(9)–N(2)–C(8)	116.90(13)

Average C–C distance in the phenyl ring 1.390 Å [1.383(2)–1.396(2) Å]. Average C–C–C angle in the phenyl ring 120.0° [119.45(13)–120.79(14)°].

Table 3 Selected distances (Å) and bond angles (°) of $[\{Cu(PPh_3)_2\}_2(\mu\text{-bpip})][BF_4]_2$ in the crystal

Cu(1)–N(2)	2.085(4)	N(2)–C(8)	1.348(6)
Cu(1)–N(1)	2.101(4)	N(2)–C(9)	1.349(6)
Cu(1)–P(1)	2.2666(15)	C(71)–C(7)	1.502(7)
Cu(1)–P(2)	2.2741(14)	C(7)–C(8)	1.506(7)
N(1)–C(7)	1.281(6)	C(8)–C(9A)	1.384(7)
N(1)–C(6)	1.448(6)		
N(2)–Cu(1)–N(1)	78.0(2)	C(9)–N(2)–Cu(1)	128.9(3)
N(2)–Cu(1)–P(1)	109.39(12)	C(1)–C(6)–C(5)	120.2(5)
N(1)–Cu(1)–P(1)	122.56(12)	C(1)–C(6)–N(1)	120.2(5)
N(2)–Cu(1)–P(2)	121.89(11)	C(5)–C(6)–N(1)	119.6(5)
N(1)–Cu(1)–P(2)	109.95(11)	N(1)–C(7)–C(71)	126.3(5)
P(1)–Cu(1)–P(2)	111.95(5)	N(1)–C(7)–C(8)	114.6(4)
C(7)–N(1)–C(6)	117.7(4)	C(71)–C(7)–C(8)	119.1(4)
C(7)–N(1)–Cu(1)	116.9(3)	N(2)–C(8)–C(9A)	121.6(4)
C(6)–N(1)–Cu(1)	125.1(3)	N(2)–C(8)–C(7)	115.8(4)
C(8)–N(2)–C(9)	116.3(4)	C(9A)–C(8)–C(7)	122.5(4)
C(8)–N(2)–Cu(1)	114.0(3)	N(2)–C(9)–C(8A)	122.0(5)

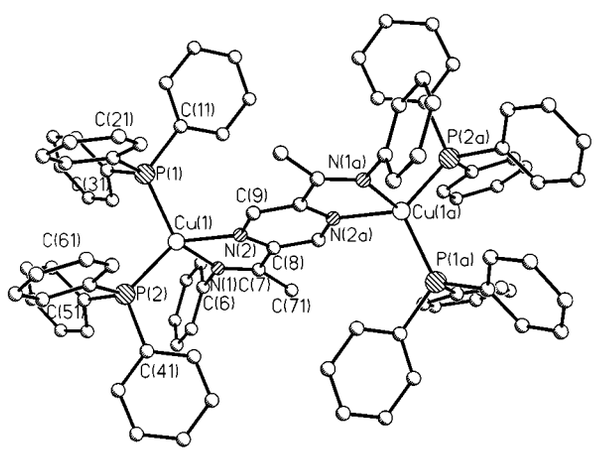

Fig. 2 Molecular structure of the complex dication in the crystal of $[\{Cu(PPh_3)_2\}_2(\mu\text{-bpip})][BF_4]_2$.

The existence of rotamers **I**–**III** (Scheme 1) has been inferred previously for the one-electron reduced $(bpip)^{\bullet -}$ from EPR and ENDOR (electron nuclear double resonance) studies;[11] in agreement with calculations (see below), conformations close to **I** have the advantage of non-interference between the methyl groups and the pyrazine protons.[11]

The dicopper complex with a metal-metal distance of 6.944 Å exhibits the typical co-ordination of copper(I) centres in an N_2P_2 donor setting,[22,23] *i.e.* distorted tetrahedral symmetry. The bond lengths to both P atoms are rather similar as are both Cu–N distances (slightly shorter for the bond to pyrazine N, Table 3). As has been demonstrated before,[2c] the stronger donation from one nitrogen centre (here pyrazine N) may be compen-

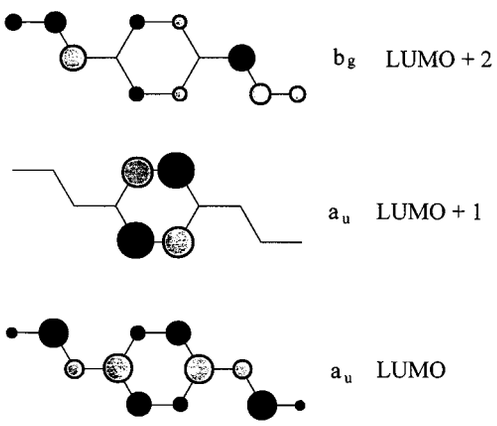

Fig. 3 π Molecular orbital representations of DFT calculated virtual MOs of bpip (*syn*/*trans*/*syn* conformation, methyl and phenyl groups not depicted).

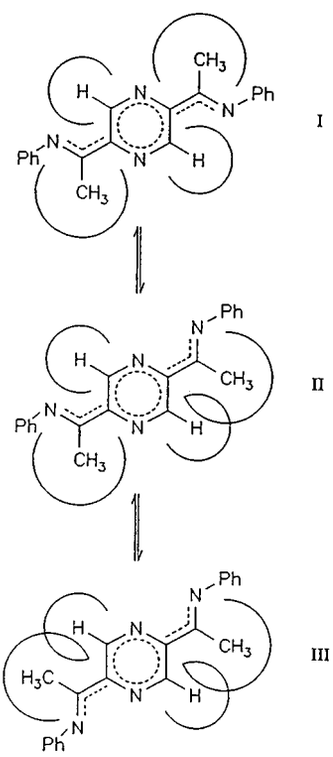

Scheme 1

sated by the better π acceptor capacity and thus stronger back bonding capability of the other centre (here imine N). The overall π back donation from both copper(I) centres to the bpip ligand is weak as illustrated by the regular C=N and C–C bond lengths (Table 3).[24]

Ab initio Hartree–Fock (HF) and density functional DFT/HF hybrid methods[25] were used in calculations of bpip and bpip′. Geometry optimisation within constrained C_i symmetry led to an *anti*/*trans*/*anti* conformation of the bpip central π system with tilted (55.5°) phenyl rings. Local minima were also observed for *syn*/*trans*/*syn* and *syn*/*trans*/*anti* rotamer situations (Scheme 1) where the tilt angle to the phenyl rings is lower than 55°. The calculation results and the experimental values from the crystal structure analysis of bpip show very good agreement (Table 4). As mentioned before, the bond parameters of bpip in the dicopper complex are also rather similar despite the different, co-ordination-induced conformation in the latter; the main difference concerns the slightly longer bond C(6)–N(1) due to the orthogonality between the phenyl ring and the imine function which precludes π conjugation.

The DFT calculations of one-electron orbitals yield the

Table 4 Selected experimental and calculated structural data[a] for the bpip ligand

	bpip		Exptl. for dicopper complex[c]
	Exptl.	Calc.[b]	
C(6)–N(1)	1.419(2)	1.407	1.448(6)
C(7)–N(1)	1.279(2)	1.287	1.281(6)
C(7)–C(8)	1.489(2)	1.497	1.506(7)
C(7)–C(71)	1.501(2)	1.512	1.502(7)
C(8)–N(2)	1.336(2)	1.347	1.348(6)
N(2)–C(9)	1.331(2)	1.334	1.349(6)
C(8)–C(9A)	1.392(2)	1.410	1.384(7)
N(1)–C(7)–C(8)	116.00(13)	116.3	114.6(4)
N(1)–C(7)–C(71)	127.10(13)	127.2	126.3(5)
C(7)–C(8)–N(2)	117.33(13)	117.8	115.8(4)
N(2)–C(9)–C(8A)	122.69(13)	122.2	122.0(5)
C(9)–N(2)–C(8)	116.90(13)	117.3	116.3(4)

[a] Bond lengths (Å) and angles (°). [b] For *anti*/*trans*/*anti* conformation from DFT calculations on bpip. [c] For *syn*/*trans*/*syn* conformation.

Table 5 Changes of the DFT calculated bond lengths (Å) of bpip′ after electron uptake

	bpip′	$(bpip')^{\bullet -}$	$(bpip')^{2-}$
C(6)–N(1)	1.407	1.387	1.359
C(7)–N(1)	1.285	1.318	1.347
C(7)–C(8)	1.502	1.433	1.405
C(8)–N(2)	1.347	1.380	1.418
N(2)–C(9)	1.335	1.318	1.307
C(8)–C(9A)	1.410	1.429	1.448

energies and compositions of the π acceptor MOs which are shown in Fig. 3. While the highest lying occupied MOs are formed by combinations of nitrogen lone pairs and phenyl orbitals, the lowest-lying unoccupied molecular orbitals (LUMO, LUMO + 1) are two π MOs of a_u symmetry (Fig. 3), one lower-lying MO with strong imine contribution (π^*_1, LUMO) and one MO centred at the pyrazine ring (π^*_2). Depending on the conformation of the phenyl rings, the b_g π MO with large phenylimino contributions may come to lie slightly lower than π^*_2, especially in a coplanar arrangement.

The geometry change as a function of electron addition has been calculated by example of bpip′ (Table 5). As illustrated by resonance structures for the dianion of the bpip chromophore, the reduction of bpip′ leads to an increase of bond orders for C(6)–N(1), C(7)–C(8) and N(2)–C(9) and to bond lengthening (decreasing bond order) for C(7)–N(1), C(8)–N(2) and C(8)–C(9). Electron acquisition also diminishes the optimum torsional angle C(7)–N(1)–C(6)–C(1) from 34.3 *via* 28.1° for $(bpip')^{\bullet -}$ to 8.3° for $(bpip')^{2-}$, reflecting increasing π conjugation with the phenyl rings. Clearly, the addition of space-demanding methyl groups on going from bpip′ to bpip results in a larger tilt angle for the phenyl rings (34.3 to 55.5°, both calculated; experimental value 54.9°).

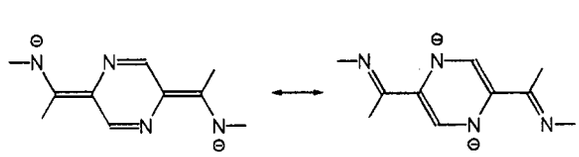

Electrochemistry

Two typical cyclic voltammograms of bpip complexes are shown in Figs. 4 and 5; the results are listed in Table 6. The ligand bpip and its complexes are reduced reversibly at potentials which are somewhat less negative (0.1–0.4 V) than those of corresponding 2,5-dpp systems.[4b] (Potentials *vs.* SCE[4b] are converted into values *vs.* ferrocene–ferrocenium by subtracting *ca.*

Table 6 Electrochemical data[a] of bpip and its complexes

Compound	$E_{1/2}$ ox II	ox I	red I	red II	Solvent
bpip			−2.05 (80)	−2.39 irr.[b]	THF
			−1.87 (70)	−2.28 irr.[b]	MeCN
[{Cr(CO)$_4$}$_2$(μ-bpip)]		0.13 (230)[c]	−1.07 (150)	−1.84 (180)	THF
[{Mo(CO)$_4$}$_2$(μ-bpip)]			−1.06 (83)	−1.70 (103)	THF
[{W(CO)$_4$}$_2$(μ-bpip)]			−0.86 (160)	−1.58 (190)	THF
[{Mn(CO)$_3$Cl}$_2$(μ-bpip)]			−0.78 (150)	−1.39 irr.[b]	THF
[Re(bpip)(CO)$_3$Cl]		1.12 irr.[d]	−1.17 (117)	−1.89 irr.[b]	THF
[{Re(CO)$_3$Cl}$_2$(μ-bpip)]			−0.54 (200)	−1.30 (200)	THF
		1.00 irr.[d]	−0.60 (60)	−1.27 (130)	MeCN
[{Cu(PPh$_3$)$_2$}$_2$(μ-bpip)][BF$_4$]$_2$		1.02 irr.[d]	−0.75 (63)	−1.52 (153)	CH_2Cl_2
		0.92 irr.[d]	−0.92 (96)	−1.48 (63)	MeCN
[{Ru(bpy)$_2$}$_2$(μ-bpip)][PF$_6$]$_4$	<1.09 (69)	1.01 (69)	−0.63 (69)	−1.26 (72)[e]	MeCN

[a] From cyclic voltammetry at 100 mV s^{-1} scan rate. Potentials in V *vs.* ferrocene–ferrocenium couple. Half-wave potentials $E_{1/2}$, peak potential differences $\Delta E_p = E_{pa} - E_{pc}$ in mV in parentheses. [b] Cathodic peak potential E_{pc} for irreversible reduction step. [c] Two-electron wave. [d] Anodic peak potential E_{pa} for irreversible oxidation step. [e] Additional bpy-centred reduction at −1.75 V.

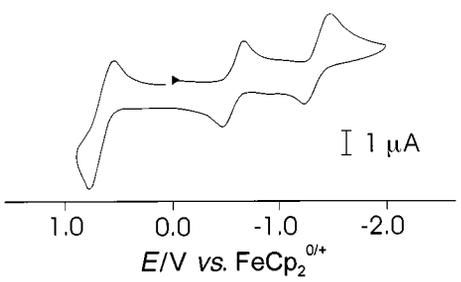

Fig. 4 Cyclic voltammogram of [{Cr(CO)$_4$}$_2$(μ-bpip)] in THF–0.1 M Bu_4NClO_4 at 100 mV s^{-1} scan rate.

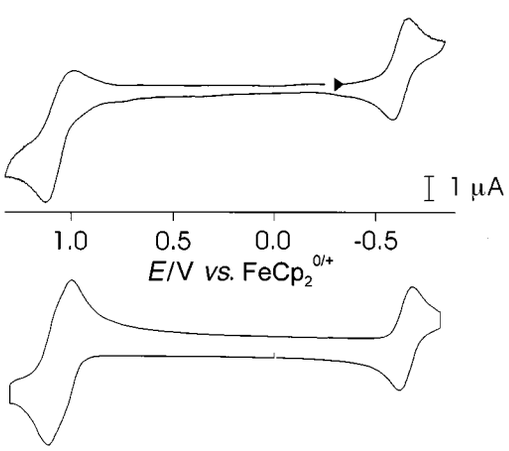

Fig. 5 Experimental and simulated cyclic voltammograms of [{Ru(bpy)$_2$}$_2$(μ-bpip)][PF$_6$]$_4$ in MeCN–0.1 M Bu_4NPF_6.

0.45 V.[26]) Substitution of the 2-pyridyl by two *N*-phenylimine functions clearly causes an energetic stabilisation of the LUMO and thus of reduced forms. Under the conditions employed, the second reduction is irreversible for the 'free' ligand and the halide containing species; otherwise, a difference of about 0.7 V is observed between first and second reversible reductions.

Facilitated reduction of π acceptor ligands after single and especially twofold metal co-ordination is a well known phenomenon,[4b,19,21] the increase in half-wave reduction potentials $E_{1/2redI}$ from the 'free' ligand *via* the complexes of Cr^0, Mo^0, W^0, Mn^I, Cu^I, Ru^{II} to the rhenium(I) dinuclear complex follows corresponding sequences for related complexes with bis(chelating) bridging ligands.[19,20b]

As expected for compounds with metal centred HOMOs, the oxidation of the complexes proceeds irreversibly except for the dichromium(0) and diruthenium(II) systems. In both instances, however, this metal-based oxidation occurs as a virtual two-electron process (Fig. 4), with only indirectly detectable formation of a Ru^{III}–Ru^{II} mixed-valent intermediate form (Fig. 5). The comproportionation constant K_c for the mixed-valent form is $10^{3.2}$ for the [{Ru(bpy)$_2$}$_2$(μ-2,5-dpp)]$^{5+}$ reference[27] but less than $10^{1.4}$ for [{Ru(bpy)$_2$}$_2$(μ-bpip)]$^{5+}$, see eqns. (1) and (2).

$$K_c = 10^{\Delta E/59\ mV} = [X^{(n-1)}]^2/[X][X^{(n-2)}] \quad (1)$$

$$X + X^{(n-2)} \rightleftharpoons 2\ X^{(n-1)} \quad (2)$$

Usually, the better π acceptor bridging ligand (here bpip) should induce a stronger metal–metal coupling in terms of stability of mixed-valent states[27] than a weaker π acceptor (here 2,5-dpp), especially if the metal–metal distances are comparable. The unexpected deviation from this rule[27] as observed here is attributed to the predominantly imine-centred π^*_1 MO for metal–metal communication (Fig. 3); the metals thus mainly interact with the *peripheral* acceptor part of the bridging ligand. In contrast, the mediating π^*_1 MO of 2,5-dpp has the main acceptor functionality in the *central* pyrazine ring,[4b] and similar situations are found for all related bridging ligands.[4b] Nevertheless, the bpip bridging ligand has been unique in allowing us to observe the uncommon d^7/d^8 mixed-valent state of complexes [(C_5Me_5)M(μ-bpip)M(C_5Me_5)]$^+$, M = Rh or Ir.[9]

UV/VIS spectroscopy, solvatochromism and spectroelectrochemistry

Complexes between π acceptor ligands and metal centres in low oxidation states are usually distinguished by intense, low-energy and often highly solvatochromic[28–30] metal-to-ligand charge transfer (MLCT) transitions. Table 7 summarises the solvent dependence of the long-wavelength MLCT absorption for the carbonylmetal compounds and Table 8 contains additional information for some reduced systems from spectroelectrochemistry (Fig. 6).

In comparison with corresponding 2,5-dpp compounds,[4b,19,21] all dinuclear bpip complexes exhibit first MLCT absorption bands (MLCT1, d ⟶ π^*_1) at distinctly longer wavelengths. The reason for this bathochromic shift, *e.g.* from 584 [650 (sh)] to 721 [800 (sh)] nm for the dinuclear bis(2,2′-bipyridine)-ruthenium(II) complexes, lies in the lower lying LUMO of bpip compounds relative to 2,5-dpp systems which is evident from facilitated reduction (Table 6). The occupied metal d orbitals, on the other hand, have about the same energy in bpip and 2,5-dpp complexes as illustrated by comparative absolute potentials

Table 7 Solvent dependent MLCT[a] absorption maxima λ_{max}/nm of dinuclear carbonyl metal complexes of L = μ-bpip and solvatochromism parameters[b]

Solvent	E^*_{MLCT}[c]	[{Cr(CO)$_4$}$_2$L]	[{Mo(CO)$_4$}$_2$L]	[{W(CO)$_4$}$_2$L]	[{Mn(CO)$_3$Cl}$_2$L]	[{Re(CO)$_3$Cl}$_2$L]
Hexane	0.00	Insoluble	Insoluble	Insoluble	382	Insoluble
					642	
Toluene	0.30	513	482		376	395
		862	817	820	635	651
Benzene	0.34	519	488		377	395
		858	808	823	636	649
THF	0.59	490	460	440	364 (sh)	376 (sh)
		817	765	787	640	603
DCE[d]	0.64	510	475		376	378
		836	790	800	639	636
Acetone	0.82	475	452 (sh)	427 (sh)	362 (sh)	366
		785	734	759	635	584
MeCN	0.90	463	450		362	368
		771	715	749	634	578
DMF	0.95	450	44 (sh)		360 (sh)	
		766	715	741	628	567
A_1[b]		10950	11470	11510	15610	14350
B_1		2150	2640	2050	220	3420
A_2		18060	19600	Insufficient	26130	24220
B_2		4030	3330	data	1770	3500

[a] Metal-to-ligand charge transfer to π_1* (LUMO; MLCT1) and π_2* (SLUMO; MLCT2). [b] Solvatochromism analysed *via* linear regressions $\tilde{\nu}_{MLCTn}$/cm^{-1} = $A_n + B_nE^*_{MLCT}$. [c] Solvent parameter from ref. 28. [d] 1,2-Dichloroethane.

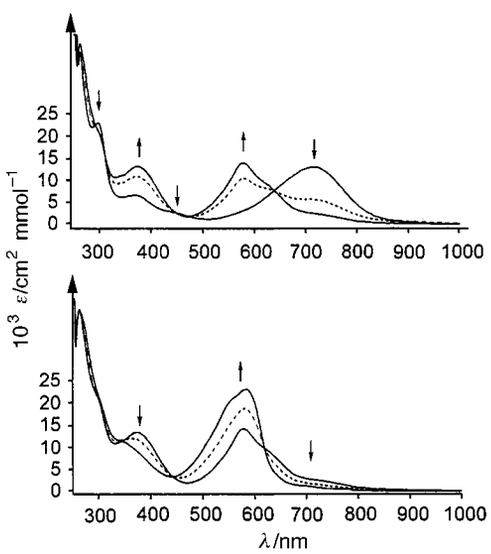

Fig. 6 Absorption spectra of [{Mo(CO)$_4$}$_2$(μ-bpip)]^n from spectroelectrochemistry in DMF–0.1 M Bu_4NPF_6. Top: n = 0 to −1. Bottom: n = −1 to −2.

for the $Ru^{II} \longrightarrow Ru^{III}$ oxidation (Table 6, ref. 21). The stronger acceptor effect of bpip relative to 2,5-dpp is also evident[21] from the hypsochromically shifted d ⟶ π*(bpy) absorption of [{Ru(bpy)$_2$}$_2$(μ-bpip)]$^{4+}$ (422 nm) relative to the 432 nm of [{Ru(bpy)$_2$}$_2$(μ-2,5-dpp)]$^{4+}$.[21]

The typically[29,30] negative solvatochromism of MLCT absorptions of d^6 metal carbonyl complexes has been quantified using the well established[30] E^*_{MLCT} solvent parameters as defined by Manuta and Lees.[28] Linear correlations were observed in all cases, and the values of the regressions $\nu_{MLCT} = A + BE^*_{MLCT}$ are listed in Table 7 for MLCT1 and MLCT2 bands. The A_1 values reflect the established[4b,19] sequence of MLCT1 energies, increasing from compounds of Cr^0 *via* Mo^0 and W^0 to Re^I and Mn^I. The sensitivity as measured by B_1 shows large differences; the manganese(I) dimer shows almost no solvent dependence whereas the rhenium(I) analogue exhibits rather large hypsochromic shifts with increasing solvent polarity. This contrast suggests[30b] that σ donation and π acceptance through the ligand are more balanced in the dimanganese(I) compound.

Table 8 Spectroelectrochemical data:[a] UV/VIS absorption of bpip and its complexes

Compound	λ/nm (10^{-3} ε/M^{-1} cm^{-1})
bpip	291 (23.7), 365 (sh) (5.5)
bpip$^{\cdot-}$	240 (13.7), 280 (16.9), 460 (13.2), 700 (5.1)
bpip^{2-}	245 (19.5), 272 (11.3), 469 (27.1)
[{Mo(CO)$_4$}$_2$(μ-bpip)][b]	298 (23.0), 386 (6.5), 450 (2.5), 715 (13.0)
[{Mo(CO)$_4$}$_2$(μ-bpip)]$^{\cdot-}$[b]	368 (13.0), 577 (14.0), 625 (sh), 715 (sh)
[{Mo(CO)$_4$}$_2$(μ-bpip)]$^{2-}$[b]	343 (sh), 554 (20.0), 583 (23.0)
[{Cu(PPh$_3$)$_2$}$_2$(μ-bpip)]$^{2+}$	267 (48.6), 392 (3.9)
[{Cu(PPh$_3$)$_2$}$_2$(μ-bpip)]$^{+}$	274 (48.0), 440 (12.6), 500 (10.9), 622 (10.1), 879 (0.15)
[{Cu(PPh$_3$)$_2$}$_2$(μ-bpip)]	254 (44.5), 538 (sh) (35.1), 565 (40.2), 716 (1.64)

[a] From measurements in MeCN unless stated otherwise. For assignments of transitions see text. Reduced forms generated by *in situ* electrolysis in solvent–0.1 M Bu_4NPF_6 at ambient temperatures. [b] Measured in DMF.

A comparison between [{Mo(CO)$_4$}$_2$(μ-bpip)] and [{Mo(CO)$_4$}$_2$(μ-2,5-dpp)][30a] reveals that the former exhibits a lower A_1 value (11470 *vs.* 13360 cm^{-1}) and a diminished sensitivity B_1 (2640 *vs.* 3110 cm^{-1}), confirming once again the better π acceptor capacity of bpip relative to 2,5-dpp.

The 'free' ligand and the complexes of the Mo^0 and the Cu^I were studied in their singly and doubly reduced forms by UV/VIS spectroelectrochemistry (Fig. 6, Table 8). The ions bpip$^{\cdot-}$ and bpip^{2-} show absorptions in the visible due to transitions from the singly or doubly occupied π^*_1 MO to higher lying unoccupied orbitals.[31] New bands at longer wavelengths are also observed for the dicopper(I) complex, where intraligand (IL) and MLCT transitions are expected. The dimolybdenum(0) complex, on the other hand, exhibits a long-wavelength MLCT1 band in the neutral form; on reduction this band is shifted hypsochromically (anion radical) and then disappears (dianion) whereas other, intraligand transitions dominate.

EPR spectroscopy of reduced forms

The magnetic resonance behaviour of the bpip radical anion was previously reported.[11] Temperature-dependent EPR and ENDOR studies revealed a dynamic situation resulting from

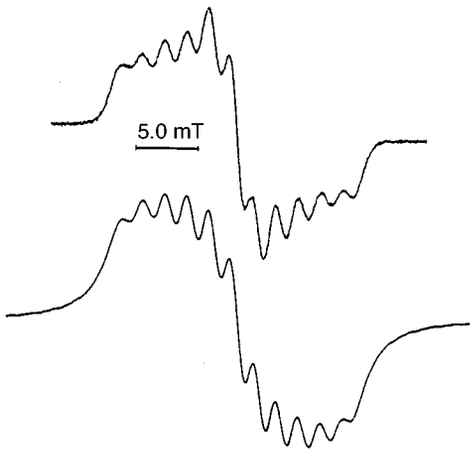

Fig. 7 The EPR spectrum of $[\{Re(CO)_3Cl\}_2(\mu\text{-bpip})]^{\bullet -}$ in acetone solution with computer simulation (linewidth 1.93 mT).

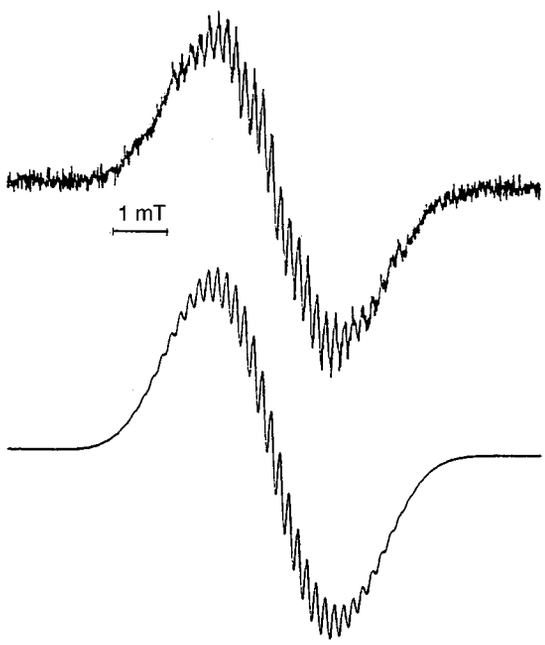

Fig. 8 The EPR spectrum of $[\{Cu(PPh_3)_2\}_2(\mu\text{-bpip})]^{\bullet +}$ in acetone solution with computer simulation (linewidth 0.43 mT).

restricted rotation around the C (imine)–C (pyrazine) bonds (Scheme 1).

The one-electron reduced forms of the dinuclear complexes also exhibit EPR spectra at ambient temperature (Figs. 7 and 8), and the *g* values and hyperfine constants are summarised in Table 9. The dinuclear manganese(I) complex showed only a broad, unresolved signal on reduction.

The EPR data are compatible with results from related anion radical complexes $(L_nM)(BL^{\bullet -})(ML_n)$.[8,19,20b,32] This concerns the decrease of *g* values from the tungsten(0) complex *via* Cu^{I}, Mo^{0}, Cr^{0} and Re^{I} to Ru^{II}, the detection of sizeable metal hyperfine splitting for $^{63,65}Cu$, $^{95,97}Mo$ and $^{185,187}Re$, and the strong increase, in fact more than doubling, of the ^{14}N coupling constants after metal binding. Remarkably, the hyperfine coupling from the chemically different imine and pyrazine nitrogen donor atoms is identical for the ligand *and* complex radical species within the respective EPR linewidths. This observation agrees with results from Hückel MO calculations of π spin populations;[11] the DFT calculations suggest slightly higher MO coefficients at the imine nitrogen centres in the LUMO (Fig. 3).

Summarising, the conjugated π system underlying the bpip bridging ligand is causing several unexpected effects in dinuclear complexes such as the stabilisation of d^7/d^8 and the poor support of d^5/d^6 mixed-valent states; the structural and electronic potential of this kind of species thus deserves to be explored further.

Table 9 The EPR data[a] of paramagnetic species

Compound	g_{iso}	a_M	a_N[c]
$bpip^{\bullet -}$[b]	2.0033		0.159
$[\{Cr(CO)_4\}_2(\mu\text{-bpip})]^{\bullet -}$[d]	2.0021	n.o.	0.339
$[\{Mo(CO)_4\}_2(\mu\text{-bpip})]^{\bullet -}$[d]	2.0029	0.247 ($^{95,97}Mo$)	0.335
$[\{W(CO)_4\}_2(\mu\text{-bpip})]^{\bullet -}$[d]	2.0036	n.o.	0.330
$[\{Re(CO)_3Cl\}_2(\mu\text{-bpip})]^{\bullet -}$[d]	2.0005	1.74 ($^{185,187}Re$)	n.o.
$[\{Cu(PPh_3)_2\}_2(\mu\text{-bpip})]^{\bullet +}$[e]	2.0030	1.32 ($^{63,65}Cu$; ^{31}P)	0.34
$[\{Ru(bpy)_2\}_2(\mu\text{-bpip})]^{\bullet 3+}$[d,f]	1.9980	n.o.	n.o.

[a] Coupling constants *a* in mT (1 T = 10^4 G). [b] Generated by *in situ* electrolysis at ambient temperatures in THF–0.1 M Bu_4NClO_4. [c] Within the linewidth the ^{14}N hyperfine splitting was found identical for imine and azine nitrogen centres. [d] Generated by reduction with Bu_4NBH_4 in acetone. [e] Generated by reduction with Bu_4NBH_4 in CH_2Cl_2. [f] *g* Components at 1.979, 1.996, 2.019 in acetone at 110 K.

Experimental

Instrumentation

The EPR spectra were recorded in the X band on a Bruker System ESP 300 equipped with a Bruker ER035M gaussmeter and a HP 5350B microwave counter, ^1H NMR spectra on a Bruker AC 250 spectrometer, infrared spectra using Perkin-Elmer 684 and 283 instruments and UV/VIS/NIR absorption spectra on Shimadzu UV160 and Bruins Instruments Omega 10 spectrophotometers. Cyclic voltammetry was carried out using a three-electrode configuration (glassy carbon electrode, platinum counter electrode, Ag–AgCl or SCE reference) and a PAR 273 potentiostat and function generator. The ferrocene–ferrocenium couple served as reference. Cyclic voltammograms were simulated with the help of the program DigiSim 2.1 (Bioanalytical Systems Inc., V 2.1, 1996). Spectroelectrochemical measurements were performed using an optically transparent thin-layer electrode (OTTLE) cell[33] for UV/VIS spectra and a two-electrode capillary for EPR studies.[8]

Preparations

The compound bpip was synthesized as described.[11]

$[\{Cr(CO)_4\}_2(\mu\text{-bpip})]$. The $[Cr(THF)(CO)_5]$ complex as generated by 3 h irradiation of $[Cr(CO)_6]$ (70 mg, 0.318 mmol) in 70 cm^3 THF was treated with 50 mg (0.159 mmol) bpip to yield a green solution. After stirring for 20 h the volume was reduced by half and 40 cm^3 *n*-hexane were added to precipitate the dark green product. Yield: 41 mg (40%) (Found: C, 51.31; H, 3.27; N, 8.13. Calc. for $C_{28}H_{18}Cr_2N_4O_8 \cdot H_2O$: C, 50.87; H, 3.03; N, 8.48%).

$[\{Mo(CO)_4\}_2(\mu\text{-bpip})]$. A solution of the norbornadiene complex $[Mo(nbd)(CO)_4]$ (60 mg, 0.20 mmol) in 30 cm^3 THF was treated with 30 mg (0.096 mmol) bpip to yield a deep blue solution. After stirring for 20 h 40 cm^3 *n*-hexane were added to precipitate the dark blue product which was washed with *n*-hexane and dried under vacuum. Yield: 57 mg (74%) (Found: C, 45.74; H, 2.68; N, 7.50. Calc. for $C_{14}H_9MoN_2O_4$: C, 46.05; H, 2.48; N, 7.67%). ^1H NMR (THF-d_8): δ 2.46 (s, 6 H, CH_3), 7.13 (dd, 4 H, *o*-H), 7.34 (tt, 2 H, *p*-H), 7.54 (m, 4 H, *m*-H) and 9.66 (s, 2 H, pyrazine H).

$[\{W(CO)_4\}_2(\mu\text{-bpip})]$. The $[W(THF)(CO)_5]$ complex as generated by 3 h irradiation of $[W(CO)_6]$ (112 mg, 0.318 mmol) in 70 cm^3 THF was treated with 50 mg (0.159 mmol) bpip to yield a

deep blue solution. After heating to reflux for 1 h the volume was reduced by half and 40 cm^3 *n*-hexane were added to precipitate the dark blue product. Yield: 48 mg (34%) (Found: C, 34.73; H, 3.24; N, 5.50. Calc. for $C_{14}H_9N_2O_4W \cdot 2H_2O$: C, 34.36; H, 2.66; N, 5.78%).

[{Mn(CO)$_3$Cl}$_2$(μ-bpip)]. A solution of [Mn(CO)$_5$Cl] (73.3 mg, 0.318 mmol) in 30 cm^3 THF was treated with 50 mg (0.159 mmol) bpip to yield a dark red solution. After heating to reflux for 2 h the solution had turned blue; 30 cm^3 *n*-hexane were added to precipitate the dark blue product which was washed with *n*-hexane and dried under vacuum. Yield: 56 mg (53%) (Found: C, 45.67; H, 2.87; N, 8.00. Calc. for $C_{26}H_{18}Cl_2Mn_2N_4O_6 \cdot H_2O$: C, 45.81; H, 2.94; N, 8.22%).

[{Re(CO)$_3$Cl}$_2$(μ-bpip)]. A solution of [Re(CO)$_5$Cl] (72 mg, 0.20 mmol) in 50 cm^3 toluene was treated with 31 mg (0.10 mmol) bpip to yield a dark red solution which turned purplish blue after heating to reflux for 1 h. To complete the precipitation 50 cm^3 *n*-hexane were added; the dark blue product was washed with toluene and *n*-hexane and dried under vacuum. Yield: 80 mg (86%) (Found: C, 34.32; H, 1.98; N, 5.58. Calc. for $C_{13}H_9ClN_2O_3Re$: C, 33.73; H, 1.96; N, 6.05%). ^{1}H NMR (acetone-d$_6$): δ 2.58 (s, 6 H, CH_3), 7.24 (dd, 4 H, *o*-H), 7.45 (tt, 2 H, *p*-H), 7.63 (m, 4 H, *m*-H) and 9.60 (s, 2 H, pyrazine H).

[Re(bpip)(CO)$_3$Cl]. A solution of [Re(CO)$_5$Cl] (92 mg, 0.255 mmol) in 30 cm^3 toluene–dichloromethane (3:1) was treated with 80 mg (0.255 mmol) bpip under reflux for 1 h to yield a dark red solution. The solution was cooled to 4 °C for 20 h to precipitate the purplish blue dinuclear compound. After filtration the solvent was removed *in vacuo* and the red residue recrystallised from 20 cm^3 toluene–dichloromethane (3:1) to yield 100 mg (63%) (Found: C, 45.50; H, 3.48; N, 8.51. Calc. for $C_{23}H_{18}ClN_4O_3Re$: C, 44.55; H, 2.93; N, 9.04%). ^{1}H NMR (acetone-d$_6$): δ 2.45 (s, 3 H, CH_3), 2.71 (s, 3 H, CH_3), 6.99 (dd, 4 H, *o*-H), 7.19 (m, 2 H, *m*-H), 7.42 (tt, 1 H, *p*-H), 7.44 (m, 2 H, *m*-H), 7.60 (tt, 1 H, *p*-H), 9.72 (s, 1 H, pyrazine H) and 9.79 (s, 1 H, pyrazine H). UV/VIS (THF): λ_{max} = 461 and 295 nm.

[{Cu(PPh$_3$)$_2$}$_2$(μ-bpip)][BF$_4$]$_2$. A solution of [Cu(PPh$_3$)$_4$]BF$_4$ (240 mg, 0.20 mmol) in 30 cm^3 CH_2Cl_2 was treated with 31 mg (0.10 mmol) bpip to yield a purplish brown solution. After stirring for 2 h 60 cm^3 *n*-hexane were added to precipitate the purple product which was redissolved in acetone and reprecipitated with *n*-hexane. The solid formed after keeping at 0 °C for 12 h was recrystallised from methanol and dried under vacuum. Yield: 90 mg (54%) (Found: C, 65.82; H, 4.65; N, 3.16. Calc. for $C_{92}H_{78}B_2Cu_2F_8N_4P_4 \cdot CH_3OH$: C, 65.80; H, 4.83; N, 3.30%). ^{1}H NMR (acetone-d$_6$): δ 2.37 (s, 6 H, CH_3), 6.52 (dd, 4 H, *o*-H), 7.12 (tt, 2 H, *p*-H) and 7.3–9.2 (m, 66 H, *m*-H, PPh_3, pyrazine H).

[{Ru(bpy)$_2$}$_2$(μ-bpip)][PF$_6$]$_{4-x}$. In a typical experiment a solution of *cis*-[Ru(bpy)$_2$Cl$_2$]·2H$_2$O (100 mg, 0.19 mmol) in 50 cm^3 ethanol was heated together with 30 mg (0.096 mmol) bpip for 3 h to yield a red-brown solution. Following volume reduction to about 15 cm^3 a solution of 5 mg NH_4PF_6 in 50 cm^3 water was added to produce a red-brown precipitate. After washing with water the product was redissolved in acetone, filtered and reprecipitated with diethyl ether. Column chromatography (neutral alumina) of the acetone-dissolved compound with water/acetone (1:1) yielded a main brown fraction which was repeatedly dissolved in acetone, precipitated with diethyl ether and dried under vacuum. Yield: 80 mg (53%). Elemental analysis and spectroscopy revealed that the complex contained varying amounts of the one-electron reduced species [{Ru(bpy)$_2$}$_2$(μ-bpip)][PF$_6$]$_3$, depending on reaction conditions.

Table 10 Crystallographic data for bpip and its dicopper complex[a]

	bpip	[{Cu(PPh$_3$)$_2$}$_2$(μ-bpip)][BF$_4$]$_2$
Formula	$C_{20}H_{18}N_4$	$C_{92}H_{78}B_2Cu_2F_8N_4P_4$
Formula weight (*M*)	314.38	1664.16
Crystal system	Orthorhombic	Monoclinic
Space group	*Pbca* (no. 61)	$P2_1/n$ (no. 14)
a/Å	6.3013(4)	13.844(3)
b/Å	7.8308(7)	11.111(3)
c/Å	33.242(3)	26.604(6)
β/°		105.03(2)
V/Å^3	1640.3(2)	3952.20(17)
Z	4	2
μ(Mo-Kα)/mm^{-1}	0.078	0.689
Measured reflections	2370	7271
Unique data	2370	6974
Data with $I > 2\sigma(I)$	1680	4882
*R*1 [$I > 2\sigma(I)$]	0.0480	0.0622
*wR*2 (all data)	0.1449	0.1844

Crystallography

Yellowish crystals of bpip were obtained by cooling a saturated solution in toluene. Wyckoff scans and 2255 reflections were used for refinement. Crystals of [{Cu(PPh$_3$)$_2$}(μ-bpip)][BF$_4$]$_2$ were obtained as purplish black needles by slow evaporation of a saturated solution in acetone. Wyckoff scans and 6568 reflections were used for refinement.

Data were collected at 183 K on a Siemens P4 diffractometer with graphite monochromator and Mo-Kα radiation (λ 0.71073 Å). The structures were solved by direct methods (Siemens SHELXTL PC) and refined (SHELXL 93)[34] by full-matrix least squares on F^2. Hydrogen atoms were introduced at calculated positions and refined freely. Other details are given in Table 10.

CCDC reference number 186/1291.

See http://www.rsc.org/suppdata/dt/1999/575/ for crystallographic files in .cif format.

Calculations

Ab initio Hartree–Fock (HF) and density-functional (DFT)/HF hybrid[25] methods were used for electronic structure calculations of the bpip ligand. Within the DFT/HF procedure, the three-parameter Becke–Lee–Yang–Parr (B3LYP) functional potential was employed. Calculations were performed using the GAUSSIAN 94 program package.[35] Dunning's[36] valence double-ζ basis with polarisation functions was used for H, C and N atoms. The geometry variation as a function of reduction was examined for bpip′ where the methyl groups of bpip were replaced by H atoms. The calculations were done within C_i symmetry constraint.

Acknowledgements

Support of this work and German-Czech co-operation from Deutsche Forschungsgemeinschaft and Volkswagenstiftung is gratefully acknowledged.

References

1 (*a*) V. Balzani, S. Campagna, G. Denti, A. Juris, S. Serroni and M. Venturi, *Acc. Chem. Res.*, 1998, **31**, 26; (*b*) S. Bodige, A. S. Torres, D. J. Maloney, D. Tate, G. R. Kinsel, A. K. Walker and F. M. MacDonnell, *J. Am. Chem. Soc.*, 1997, **119**, 10364; (*c*) E. Constable, *Chem. Ind.* (*London*), 1994, 56; (*d*) A. Neels, B. M. Neels, H. Stoeckli-Evans, A. Clearfield and D. M. Poojary, *Inorg. Chem.*, 1997, **36**, 3402.

2 (*a*) G. De Munno, G. Viau, M. Julve, F. Lloret and J. Faus, *Inorg. Chim. Acta*, 1997, **257**, 121; (*b*) G. De Munno, T. Poerio, M. Julve, F. Lloret, J. Faus and A. Caneschi, *J. Chem. Soc., Dalton Trans.*, 1998, 1679; (*c*) W. Kaim, S. Kohlmann, J. Jordanov and D. Fenske,

Z. Anorg. Allg. Chem., 1991, **598/599**, 217; (*d*) G. Brewer and E. Sinn, *Inorg. Chem.*, 1985, **24**, 1580.
3 J. Poppe, M. Moscherosch and W. Kaim, *Inorg. Chem.*, 1993, **32**, 2640; V. Kasack, W. Kaim, H. Binder, J. Jordanov and E. Roth, *Inorg. Chem.*, 1995, **34**, 1924; M. Ketterle, J. Fiedler and W. Kaim, *Chem. Commun.*, 1998, 1701.
4 (*a*) S. Kohlmann, S. Ernst and W. Kaim, *Angew. Chem.*, 1985, **97**, 698; *Angew. Chem., Int. Ed. Engl.*, 1985, **24**, 684; (*b*) W. Kaim and S. Kohlmann, *Inorg. Chem.*, 1987, **26**, 68; (*c*) W. Kaim, S. Kohlmann, A. J. Lees, T. L. Snoeck, D. J. Stufkens and M. M. Zulu, *Inorg. Chim. Acta*, 1993, **210**, 159.
5 (*a*) L. De Cola, V. Balzani, F. Barigelletti, L. Flamigni, P. Belser, A. von Zelewsky, M. Frank and F. Vögtle, *Inorg. Chem.*, 1993, **32**, 5228; (*b*) I. S. Calonaci, Ph.D. Thesis, University of Amsterdam, 1995.
6 (*a*) H. Haga and K. Koizumi, *Inorg. Chim. Acta*, 1985, **104**, 47; S. C. F. Maloney, M. R. McDevitt and F. L. Urbach, *Inorg. Chim. Acta*, 1989, **164**, 123; (*b*) M. Krejcik, S. Zalis, J. Klima, D. Sykora, W. Matheis, A. Klein and W. Kaim, *Inorg. Chem.*, 1993, **32**, 3362; (*c*) F. Baumann, W. Kaim, M. Garcia Posse and N. E. Katz, *Inorg. Chem.*, 1998, **37**, 658; (*d*) F. Baumann, A. Stange and W. Kaim, *Inorg. Chem. Commun.*, 1998, **1**, 305.
7 C. Creutz, *Prog. Inorg. Chem.*, 1983, **30**, 1; D. E. Richardson and H. Taube, *Coord. Chem. Rev.*, 1984, **60**, 107; R. J. Crutchley, *Adv. Inorg. Chem.*, 1994, **41**, 273; W. Bruns, W. Kaim, E. Waldhör and M. Krejcik, *Inorg. Chem.*, 1995, **34**, 663.
8 W. Kaim, S. Ernst and V. Kasack, *J. Am. Chem. Soc.*, 1990, **112**, 173.
9 W. Kaim, R. Reinhardt and J. Fiedler, *Angew. Chem.*, 1997, **109**, 2600; *Angew. Chem., Int. Ed. Engl.*, 1997, **36**, 2493; W. Kaim, S. Berger, S. Greulich, R. Reinhardt and J. Fiedler, *J. Organomet. Chem.*, in the press.
10 A. Klein, S. Hasenzahl, W. Kaim and J. Fiedler, *Organometallics*, 1998, **17**, 3532.
11 T. Stahl, V. Kasack and W. Kaim, *J. Chem. Soc., Perkin Trans. 2*, 1995, 2127.
12 G. van Koten and K. Vrieze, *Recl. Trav. Chim. Pays-Bas*, 1981, **100**, 129; *Adv. Organomet. Chem.*, 1982, **21**, 152; K. Vrieze and G. van Koten, *Inorg. Chim. Acta*, 1985, **100**, 79.
13 G. van Koten, J. T. B. H. Jastrzebski and K. Vrieze, *J. Organomet. Chem.*, 1983, **250**, 49.
14 H. Brunner and W. A. Herrmann, *Chem. Ber.*, 1972, **105**, 770; *J. Organomet. Chem.*, 1973, **57**, 183.
15 D. J. Stufkens, *Coord. Chem. Rev.*, 1990, **104**, 39.
16 D. P. Drolet, L. Chan and A. J. Lees, *Organometallics*, 1988, **7**, 2502.
17 M. Maruyama, H. Matsuzawa and Y. Kaizu, *Inorg. Chem.*, 1995, **34**, 3232.
18 M. B. Lawson and E. B. Fleischer, *J. Coord. Chem.*, 1972, **2**, 79.
19 W. Kaim and S. Kohlmann, *Inorg. Chem.*, 1990, **29**, 2909.
20 (*a*) W. Kaim and S. Kohlmann, *Inorg. Chem.*, 1987, **26**, 1469; (*b*) C. Vogler and W. Kaim, *Z. Naturforsch., Teil B*, 1992, **47**, 1057.
21 S. D. Ernst and W. Kaim, *Inorg. Chem.*, 1989, **28**, 1520.
22 J. R. Kirchhoff, D. R. McMillin, W. R. Robinson, D. R. Powell, A. T. McKenzie and S. Chen, *Inorg. Chem.*, 1985, **24**, 3928.
23 C. Vogler, H.-D. Hausen, W. Kaim, S. Kohlmann, H. E. A. Kramer and J. Rieker, *Angew. Chem.*, 1989, **101**, 1734; *Angew. Chem., Int. Ed. Engl.*, 1989, **28**, 1659; C. Vogler, W. Kaim and H.-D. Hausen, *Z. Naturforsch., Teil B*, 1993, **48**, 1470.
24 S. Greulich, W. Kaim, A. Stange, H. Stoll, J. Fiedler and S. Zalis, *Inorg. Chem.*, 1996, **35**, 3998.
25 A. D. Becke, *J. Chem. Phys.*, 1993, **98**, 5648.
26 N. G. Connelly and W. E. Geiger, *Chem. Rev.*, 1996, **96**, 877.
27 S. Ernst, V. Kasack and W. Kaim, *Inorg. Chem.*, 1988, **27**, 1146.
28 C. M. Manuta and A. J. Lees, *Inorg. Chem.*, 1983, **22**, 3825.
29 E. S. Dodsworth and A. B. P. Lever, *Coord. Chem. Rev.*, 1990, **97**, 271; *Inorg. Chem.*, 1990, **29**, 499.
30 (*a*) W. Kaim and S. Kohlmann, *Inorg. Chem.*, 1986, **25**, 3306; (*b*) W. Kaim, S. Kohlmann, S. Ernst, B. Olbrich-Deussner, C. Bessenbacher and A. Schulz, *J. Organomet. Chem.*, 1987, **321**, 215.
31 P. S. Braterman, J.-I. Song, S. Kohlmann, C. Vogler and W. Kaim, *J. Organomet. Chem.*, 1991, **411**, 207; M. Krejcik, S. Zalis, M. Ladwig, W. Matheis and W. Kaim, *J. Chem. Soc., Perkin Trans. 2*, 1992, 2007.
32 W. Kaim and S. Kohlmann, *Inorg. Chem.*, 1986, **25**, 3442.
33 M. Krejcik, M. Danek and F. Hartl, *J. Electroanal. Chem. Interfacial Electrochem.*, 1991, **317**, 179.
34 G. M. Sheldrick, SHELXTL PLUS: An Integrated System for Solving, Refining and Displaying Crystal Structures from Diffraction Data, Siemens Analytical X-Ray Instruments Inc., Madison, WI, 1989; SHELXL-93, Program for Crystal Structure Determination, Universität Göttingen, 1993.
35 M. J. Frisch, G. W. Trucks, H. B. Schlegel, P. M. W. Gill, B. G. Johnson, M. A. Robb, J. R. Cheeseman, F. G. A. Keith, A. Peterson, J. A. Montgomery, K. Raghavachari, M. A. Al-Laham, V. G. Zakrzewki, J. V. Ortziz, J. V. Foresman, J. Cioslowski, B. B. Stefanov, A. Nanayakkara, M. Challacombe, C. Y. Peng, P. Y. Ayala, W. Chen, M. W. Wong, J. L. Andres, E. S. Replogle, R. Gomperts, R. L. Martin, D. J. Fox, J. S. Binkley, D. J. Defrees, J. Baker, J. P. Stewart, M. Head-Gordon, C. Gonzalez and J. A. Pople, GAUSSIAN 94, Revision B.3, Gaussian, Inc., Pittsburgh, PA, 1995.
36 T. H. Dunning, Jr. and P. J. Hay, in *Modern Theoretical Chemistry*, ed. *Electronic Structure Theory*, H. F. Schäfer III, Plenum, New York, 1977, vol. 3.

Paper 8/08293F